Available online at www.sciencedirect.com
ScienceDirect
Catalysis Today 129 (2007) 397–406
CATALYSIS TODAY
www.elsevier.com/locate/cattod

An investigation into water and thermal balance for a liquid fueled fuel processor

Marco J. Castaldi *, Federico Barrai

Earth & Environmental Engineering Department (HKSM), Columbia University, NY 10027, United States

Available online 29 September 2007

Abstract

To better understand the sizing and performance issues associated with water and energy balances of a fuel processor for a PEM fuel cell, a process flow system has been programmed into the ASPEN® simulator for a reference system supplying 600 W electrical power. The fuel processor consists of an autothermal reformer (ATR), single-stage water gas shift (WGS), dual-stage PROX reactors and an anode gas burner (AGB) operating on sulfur-free JP8. The reactor components were modeled using RGIBBS for the ATR and actual experimental kinetics for the WGS and PROX reactors. Simulations investigating thermal management, ATR and WGS performance and system efficiencies were done. Using realistic temperature approaches for heat exchangers it is likely that integrated systems will have to discard heat to the surroundings. Also, depending on the operating conditions, water will either be in surplus or deficit. At 1 atm pressure there is no condition that will enable complete water capture. The minimum pressure where water independence can be achieved is at 1.23 atm with a fuel cell utilization of 60% and a S/C = 1.5 and O/C = 1.0. The complete fuel processor is expected to be 0.46 L and 2.02 kg. This paper will expand on these findings with suggestions for optimal operating efficiencies and sizing for JP8 fuel processors.
© 2007 Elsevier B.V. All rights reserved.

Keywords: Water balance; Thermal management; Liquid fuel processor; Pressure effect

1. Introduction

The continued interest in fuel cells for many applications has typically been separated into two categories; the fuel cells themselves and the systems that will deliver the hydrogen. Currently those hydrogen delivering systems are fossil fuel based fuel processors that operate on either gaseous or liquid fuels. While there are many issues that still need to be understood and developed for liquid fuel processors, one issue that has only received limited attention thus far is the water and heat balance issues for the entire processor and fuel cell system. Until there is a reliable storage technology for pure hydrogen and renewable energy such as solar, wind or nuclear are developed, the deployment of PEM fuel cell applications will rely on hydrocarbon fuel processing for hydrogen generation. As research continues on the development of fuel cells and fuel processors, attention must be given to the thermal and water integration issues. This pertains particularly to mobile applications, but is very relevant for stationary applications if hydrocarbons are to be used. To obtain a high efficiency and relatively autonomous fuel cell power system, one must ensure a high level of thermal integration and reduce the human interactions. High efficiency makes sense and reduction of human interaction would likely lead to wide acceptance. For example, if a fuel cell system were to require the user to add water every time the system needed fuel, that would be an added burden, and could be a logistical problem, that would give all but the most enthusiastic users reason to not choose the technology. To that extent, an investigation was undertaken using an ASPEN® simulation to understand the issues associated with thermal integration and water balance for a liquid fueled fuel processor system. There have been a considerable number of studies done looking at water balance issues [1–3]. Yet, only a limited number have conducted investigations using real performance curves of the units. To provide insight into how the various units (reactors and heat exchangers) will integrate an ASPEN® flow sheet has been set up which incorporates kinetic rate expressions for the water gas shift (WGS) and preferential oxidation (PROX) reactors. In addition, real heat exchanger parameters were

* Corresponding author.
E-mail address: mc2352@columbia.edu (M.J. Castaldi).

0920-5861/$ – see front matter © 2007 Elsevier B.V. All rights reserved.
doi:10.1016/j.cattod.2006.05.090

incorporated such as the materials of construction, pressure drop, flow configuration and temperature approach. Finally, an experimental prototype system was assembled and tested under relevant conditions to ensure the ASPEN® simulation results could be achieved on an operating unit.

2. Simulation setup

A process flow diagram (PFD) was programmed in ASPEN® version 12.1 to conduct simulations over a number of parameters to gain an understanding of the factors that affect a water and thermal balance of a liquid fueled fuel processor for PEM fuel cell applications. The simulations were broken down into two broad categories—thermal balance and water balance. The first category, thermal balance simulations, explored the integration of inter-reactor heat exchangers used to preheat the reactants and cool the reformate from one reactor to the other, for example from the ATR to the WGS. The second category, water balance simulations, investigated the issues around capturing water after the fuel cell and anode gas burner. Both simulations were somewhat open ended in that ASPEN® was programmed to run multiple steam to carbon (S/C) and oxygen to carbon (O/C) ratios enabling performance trends to be examined. All calculations were carried out using conventional stream classes. For the Free-Water calculations the NBS/NRC steam table correlations were used which are typically more accurate than the default 1967 ASME steam tables. In the Property module, the base method used was IDEAL and the property method used was SRK (Souave–Redlich–Kwong equation of state). No properties were estimated, all were calculated using the appropriate equation of state. In the Flowsheeting Option module calculators were set up to adjust the PROX 1 and PROX 2 air for a pre-determined lamba (O_2/CO) which was typically 2.4 into PROX 1 and 8 into PROX 2 which was determined from prior operating experience. Finally a range of calculations were done using the Sensitivity module in the Model Analysis Tools module to generate data over a range of steam to carbon ratios and oxygen to carbon ratios. This method was preferred over the optimization calculation to investigate the performance over the desired ratios. This was done primarily because it enables trends to be observed for various operating condition changes.

Fig. 1 shows the complete PFD used in all simulations. The components of the PFD can be broken into four sections that will be further discussed below. The first section is the fuel processor; consisting of the autothermal reformer (ATR), the water gas shift reactor WGS and the PROX reactors. The second section is the fuel cell broken down into the anode and cathode as separate units. The third section is the water recovery section consisting of the anode gas burner (AGB), cathode effluent and condensing heat exchangers and finally the fourth section is the reactant delivery and inter-reactor heat exchange system.

2.1. Section one, fuel processor

The fuel processor system was programmed into ASPEN® using ideal reactors and reactions. The ATR was modeled as a RGIBBS reactor which enables simultaneous phase and

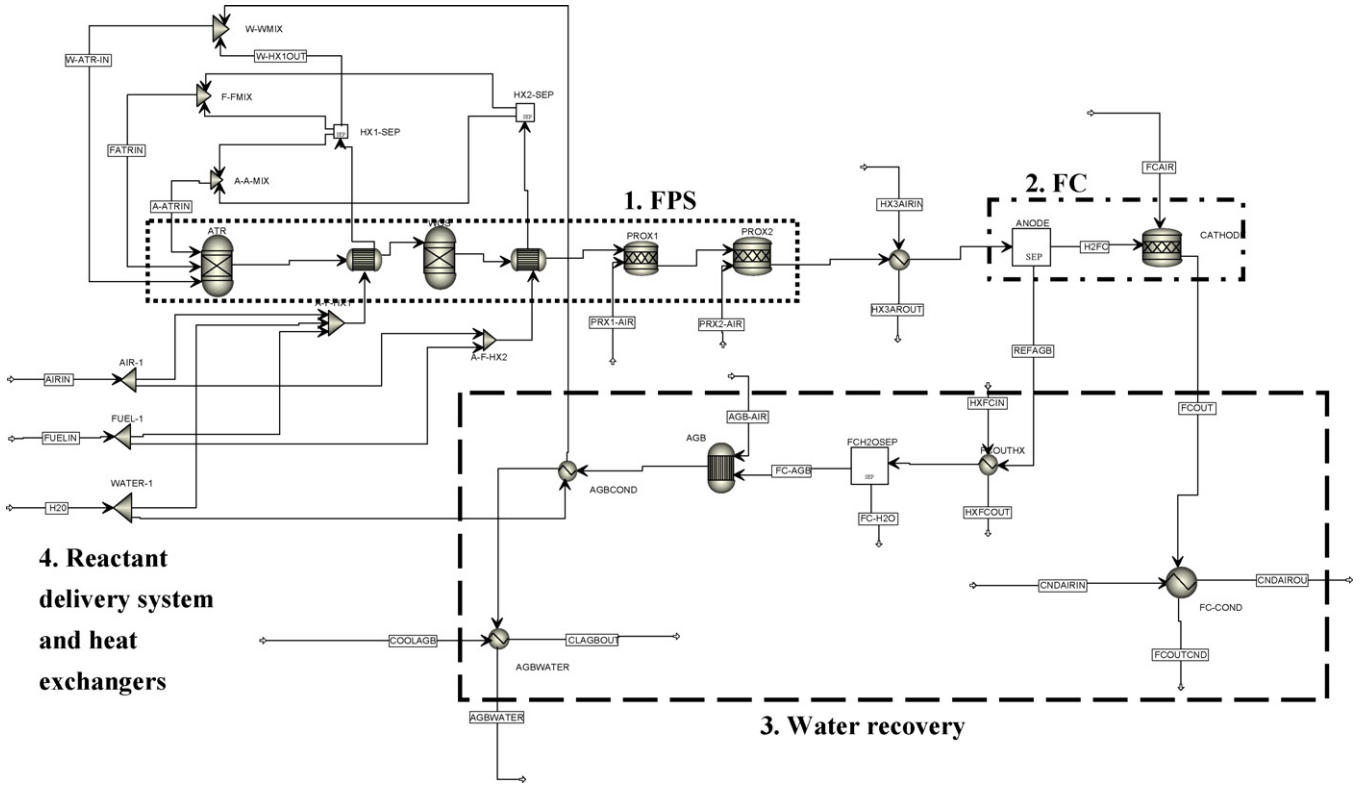

Fig. 1. Complete ASPEN process flow diagram for a liquid fueled reformer and a PEM fuel cell.

chemical equilibrium calculations to be done. The author's experience in operating liquid fueled ATR systems [4] provided the basis for the choice. Typically, one strives to have the ATR operate at equilibrium conditions to achieve the highest fuel conversion and hydrogen yield while maintaining temperatures at moderate levels. For the water balance simulations, the ATR was held at a constant inlet temperature of 250 °C and reactant operating temperature of 850 °C while the S/C and O/C ratios were varied. For the thermal simulations, the ATR inlet temperature was established by the heat exchanger between the ATR and WGS and the outlet temperature was calculated using that inlet temperature and an adiabatic equilibrium.

The WGS reactor was also modeled as an RGIBBS with constrained equilibrium. Based on operating experience and literature data [3,5] the WGS typically operates with little methanation. Therefore, the equilibrium constrained the amount of methane produced to about 100 ppm which is typical of a good WGS reactor. Again, as it has been shown with precious metal catalysts, it is possible to operate a single-stage reactor operating a moderate to low temperature (between 250 and 300 °C) [3,6–9] that can accept an inlet CO concentration of 7% and yield an outlet concentration of slightly less then 1%. It is recognized that it is unlikely the WGS will achieve equilibrium outlet compositions for all simulated conditions unless a large, i.e. low space-velocity, reactor is employed. However, for simulation purposes, the WGS reactor was allowed to achieve the constrained equilibrium compositions for all S/C and O/C variations.

The PROX reactors were modeled using RSTOIC (stoichiometric reactor unit) programmed with the CO and H_2 oxidation reactions. The selectivity toward the CO reaction was set at 45%, which has been shown by various experimentally operating systems [5,6,10,11]. Both reactors had the inlet temperatures fixed at 155°C and were operated adiabatically. The inlet air for each reactor was calculated to be twice the stoichiometric amount needed to convert all the CO, i.e. $\lambda = 4$. While this is typically on the high side, it represents an upper limit of the amount of air that would practically be introduced. Therefore, the simulation for the PROX reactors could be viewed as a worse case scenario in terms of hydrogen consumption.

2.2. Section two, fuel cell

The fuel cell for the simulation was considered a low temperature PEM unit that operated at 70 °C. The FC was broken down into two units to better model the fuel cell and facilitate the water capture calculations. The first unit was the anode which was modeled as an ideal separator, allowing only a specified amount of hydrogen to feed the cathode unit. The amount of hydrogen permitted to pass to the cathode was defined as the fuel cell utilization and was varied between 0.6 and 0.75. Based on literature values and various discussions with PEM FC manufacturers the range used in the simulations were deemed representative of many systems. The remaining hydrogen and the rest of the reformate coming from the anode went to an anode gas burner (AGB) which will be discussed in the next section. The cathode unit of the fuel cell was modeled as an RSTOIC reactor with a hydrogen oxidation reaction programmed in that enabled 99.9% conversion of the hydrogen that came from the anode. The air fed to the cathode was calculated to be twice the stoichiometric amount needed, again based on literature [13] and discussions with manufacturers. The outlet of the oxidized or combusted hydrogen and air was then sent to a condensing heat exchanger to recover the water.

2.3. Section three, water recovery system

This section consisted of mainly condensing heat exchangers and an anode gas burner (AGB). In addition, possible water recovery from the fuel cell is calculated through a condensing heat exchanger downstream of the cathode unit. The parameters used for the heat exchangers were a temperature approach of 50 K, heat rejection occurring at 50 °C, counter current flow pattern, $\Delta P/P = 10\%$, and stainless steel construction. The AGB was modeled as an RGIBBS to enable adiabatic temperature calculations and chemical species compositions.

3. Results and discussion

The primary focus of the investigation was on the fuel processor system (FPS) using JP8 fuel which has a molecular formula of $CH_{1.9}$, a density of 0.755–0.84 g/mL @ 15 °C (0.76 was used for the simulation) and a heating value of 43,147 kJ/kg. To begin to understand the operational envelope of the FPS, a thermodynamic calculation was done in the autothermal mode. This equilibrium calculation has been done by others [1,2] and is instructive to find the bounds of theoretical operation. While it does not give any insight into the practical operation of the system it does enable one to focus efforts in the right operating regime.

The general equation describing the equilibrium of any C/H/O fuel that is reacted with air and water to ideally yield carbon dioxide, hydrogen, nitrogen and any possible residual water is shown below.

$$\begin{aligned} &C_nH_mO_p + x(O_2 + 3.76N_2) + n\Psi H_2O(l) \\ &\quad \Leftrightarrow nCO_2 + (2n - 2x - p + m/2)H_2 \\ &\quad + 3.76xN_2 + [(n\Psi - (2n - 2x - p)]H_2O(g) \end{aligned}$$

For any given fuel, there are only two adjustable variables; x, which is the amount of air and Ψ, which is the amount of water. Furthermore, to obtain a thermally neutral equation, where the enthalpy of reaction is zero, once one of the variables is set the other is fixed. The results of the thermodynamic calculations for a thermo-neutral reaction are shown in Fig. 2. That is steam to carbon was varied and the equation was solved with the constraint of $\Delta H_{rxn} = 0$, which in turn fixes the O/C allowed.

The primary objective of the calculation was to find the operating regime that produced a sufficient amount of hydrogen to supply the fuel cell while ensuring that the steam

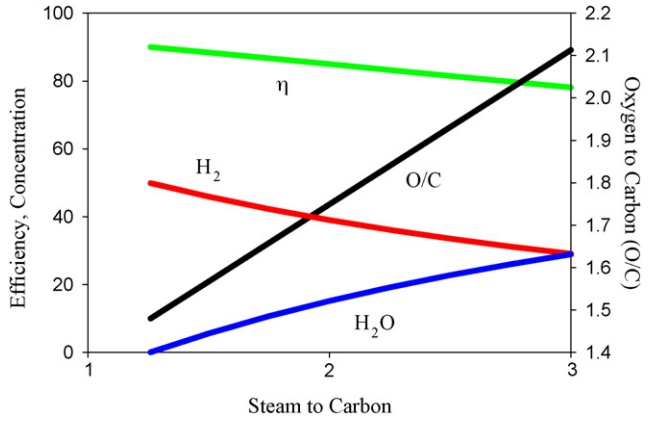

Fig. 2. Results of thermodynamic calculations from Eq. (1) for a variable steam to carbon feed.

Table 1
Results of material and energy balances for a 600 W system: comparison of energy and water needed vs. that available

	HX-1	HX-2	HX-3	AGB	Total
Energy available (kJ/min)*	13	5	3	86	107
	Fuel	Water	Air		Total
Energy needed (kJ/min)	2	14	2		18
	AGB	FC			Total
Water available (mol/min)**	0.25	0.16			0.41
	ATR feeed				
Water needed (mol/min)	0.27				

* Assuming 25 °C AGB exit temperature.
** Fuel cell anode Utilization Factor 65%.

to carbon ratio in the feed did not result in a condition where the fuel processor was water deficient. Fig. 2 shows the results of hydrogen, *excess* water concentration and efficiency, plotted on the primary ordinate and oxygen to carbon (O/C) ratio in the feed on the secondary ordinate versus steam to carbon on the abscissa. The results below S/C of about 1.25 are not shown because a realistic solution could not be found. S/C below 1.25 yields a result of negative water, which is not physically possible. That is it is not possible to thermally balance the reactions with the amount of water present. At about S/C equal to 1.25 there is just enough water fed to the reformer to balance the reaction enthalpy. Beyond an S/C of 1.25 the reformer has excess water and is shown by the blue H_2O line. Commensurate with an increase in water is a decrease in the concentration of hydrogen which directly impacts the efficiency (η), which is defined as lower heating value of hydrogen produce divided by the lower heating value of the fuel (LHV H_2/LHV JP8). The results of the calculation indicate that for highest efficiency and highest hydrogen concentration, one would operate the reformer with no excess water.

This calculation, however, does not take into account the objective of recovering water, it only identifies the parameters for minimal water usage. Combining the thermodynamic calculation described above with a material and energy balance, it is possible to calculate the theoretical potential to recover heat and water in such a system. Taking as an example, a S/C equal to 2.0 and O/C equal to 1.0 this was done for an entire 600 W system, the results of which are shown in Table 1.

For this calculation, thermodynamic equilibrium calculations were done for each reactor in the fuel processor (ATR, WGS and PROX) and a fuel cell with 65% fuel utilization with the remainder going to an anode gas burner (AGB). The material and energy balances were done to determine how much heat and water could be recovered from inter-stage heat exchangers between the fuel processor reactors. Heat exchanger 1 (HX-1) was between the ATR and WGS reactors, HX-2 was between the WGS and PROX reactors and HX-3 was between the PROX reactors and the fuel cell. Calculations indicated that there was no need for a heat exchanger between PROX 1 and PROX 2 reactors. The water recovery calculation was only done for the AGB and fuel cell exhaust because the inter-stage heat exchangers maintained outlet temperatures above 100 °C. Table 1 shows the results of this calculation. It can be seen that the energy available, recovered from the heat exchangers, is far in excess of the energy needed to raise the liquid fuel, liquid water and air to the ATR inlet temperature of 250 °C. The water balance shows that there is nearly 35% more water available in the AGB and FC exhaust than the amount needed to feed the fuel processor. Therefore, a thermodynamic calculation combined with a material and energy balance indicates that if the fuel processor operates at S/C = 2.0 and O/C = 1.0 with at 65% fuel utilization by the fuel cell it is theoretically possible to recover enough water and heat such that the system only needs to be continuously supplied air and fuel. The real question then remains, what is the practical feasibility, given the constraints of heat exchange efficiencies, water vapor pressures and size and weight constraints?

The answer to this question is addressed in detail in the ASPEN model and is further discussed below. The more complex results have to do with the water balance, thus will be discussed first. Following that, the results of the energy balance will be discussed, which basically show that in all configurations heat will have to be rejected from the system. Finally, a brief description of some experimental results is provided to demonstrate the ASPEN results are indicative of an experimental system being investigated by the authors. Fig. 1, shows a refined version of many PFD configurations. In particular the heat exchanger between the PROX and FC (HX-3) is cooled with air that is separate from the reactant air and is not used for anything in the FPS. This final version of the PFD has provisions for the water to be routed to the heat exchangers with the highest duty cycles (HX-1 and AGB exhaust). The fuel and air can be routed to the HX-1 and HX-2 only. Recall from the thermodynamic calculations that there was sufficient water recovery at S/C = 2.0 and O/C = 1.0. However, once realistic parameters for water condensation are incorporated the potential for recovery changes significantly.

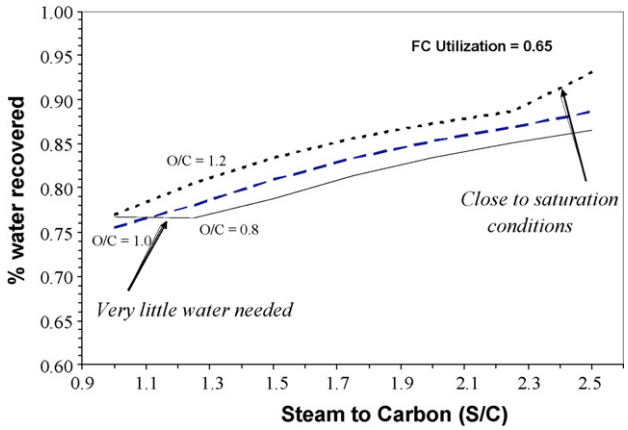

Fig. 3. Water recovery potential from ASPEN simulations.

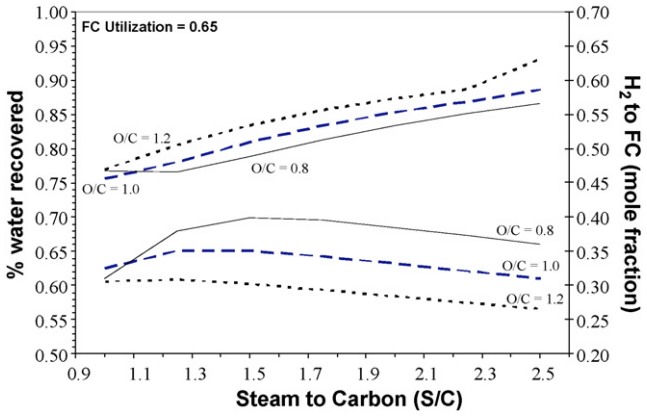

Fig. 4. Water recovery potential compared to hydrogen delivered to the fuel cell. Lower curves reference the right ordinate and upper curves reference the left ordinate.

3.1. Water balance

The simulation results for various S/C and O/C ratios, similar to the thermodynamic calculations above, are shown in Fig. 3. The figure plots %water recovered, in the liquid phase, versus S/C ratio for three different O/C ratios. It is evidenced that there is insufficient water recovery at all conditions, even high S/C values.

The results show that higher O/C ratio results in more water recovery at nearly all conditions. There is a sharp upturn in the amount recovered for O/C = 1.2 at high S/C ratio because the AGB and FC exhaust streams are getting close to saturation conditions. Not only is there a significant amount of water because of the high S/C values but also, there is an additional amount of water produced due to the high oxygen concentration entering the ATR, i.e. more combustion versus partial oxidation. The leveling off of the O/C = 0.8 curve towards the lower S/C ratios is primarily due to the comparatively lower amount of water needed. At this condition, there is only enough oxygen from the air to partially oxidize the carbon as opposed to fully oxidizing it. Therefore, there is the most CO and least amount of CO_2 formed. This in turn helps the water gas shift reaction be more effective. This combination provides a means to effectively use most of the water fed to the system to produce hydrogen as opposed to forming water in the ATR, and commensurately more CO_2, which then goes along for the ride through the rest of the fuel processor. This effective use of water manifests itself in higher hydrogen production and is shown in Fig. 4.

Fig. 4 shows the hydrogen produced in the fuel processor that is delivered to the fuel cell. For comparative purposes, the hydrogen generation is plotted on the same graph with the water recovery potential in Fig. 3. As seen in Fig. 4, at the lower S/C ratios the hydrogen generation drops precipitously for O/C = 0.8, which results in a lower amount of water usage, thus a higher recovery.

The overall trends shown in Fig. 4 are as expected with regard to low O/C yielding more hydrogen yet lower water recovery. Moreover, it provides insight into a preferred operating regime for a given objective. If the main objective is to recover water, then operation at high O/C ratios with high S/C ratios would be desirable. If however the objective is to generate hydrogen one could operate at a lower S/C and O/C producing hydrogen while sacrificing a small amount of water recovery potential. For example, operating at S/C = 1.5 and O/C = 0.8 yields approximately 15% more hydrogen with a reduction in water recovery of only 5% compared to an O/C = 1.2.

The main metric in terms of water recovery potential is the amount of water that needs to be brought compared to the amount of fuel required for a given scenario. Fig. 5 shows the pounds of water per pound of fuel over the S/C and O/C ratios examined for a fuel cell utilization of 65%. As expected, the conditions with the smallest amount of water recovery potential would require the largest amount of make-up water. In general the amount of water that is needed ranges between 0.3 and 0.42 weight fraction. Only when the recovery percentage increases significantly, i.e. above 90%, does the requirement really begin to decrease.

The amount of water needed is a result of the amount of water captured and the stoichiometry needed to reform the JP8 fuel. That is, while there is only a 5–10% change in water capture potential, the necessary make-up water varies more (~25%) due to the equilibrium constraints. The main attribute to notice is the wide range of possible S/C ratios that one could operate for any

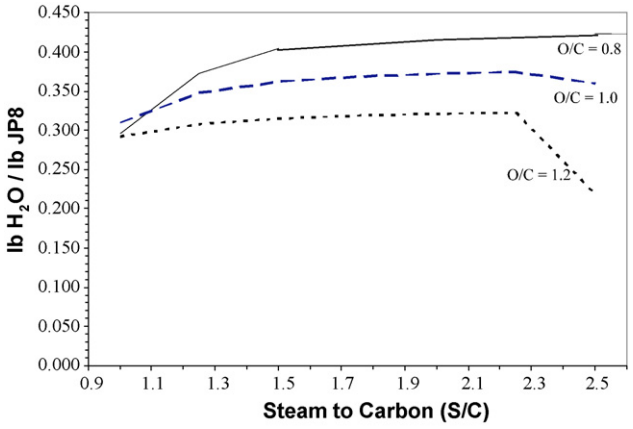

Fig. 5. Make-up water requirements for fuel cell utilization of 65%.

given O/C ratio with a given amount of water. For example, for an O/C = 1.0, a water requirement mass fraction of 0.35 enables operation over an S/C range of 1.5–2.3. As discussed above, lower O/C requires more make-up water due to the low recovery and higher O/C requires less water make because the system begins to operate near the saturation conditions.

To this point all analyses have been done with a fuel cell utilization efficiency of 65%, which is considered a representative operating regime. It is interesting to look at how the water recovery potential changes over a range of utilization rates. Fig. 6 shows how water recovery actually decreases as the fuel cell utilization increases. This is somewhat counter intuitive and would not be observed if real steam tables were not employed. That is, if a pure thermodynamic calculation is done where one assumes ideal water capture, the calculations indicate that higher fuel cell utilization would lead to higher capture potential. The results of the ASPEN simulation show this not to be the case.

Fig. 6 shows the results of the simulations over the same S/C ratios varied in other cases for an O/C = 1.0 with an operating pressure of 1 atm and operating temperature of 70 °C. The solid line is for a utilization of 70%, the dashed line is for 65% and the dot-dashed line is for 60%. In general the higher the utilization the lower the water capture potential. The issue with high utilization rates is that the amount of air needed for the cathode offsets the increase in partial pressure from higher conversion. Consequently the higher conversion removes hydrogen from the stream feeding the AGB, thus lowering the partial pressure in the AGB exhaust. The net result is an overall reduction in water capture potential. The only time higher utilization rates provide an advantage is at the high S/C ratios. It should be noted that a higher water recovery rate at lower utilization values does not necessarily translate into lower make-up water requirements. Lower utilization values require that more fuel be fed to the fuel cell to obtain the same power output. Accordingly, the water feed must be increased proportionately. This is seen in Fig. 5 for a 0.65 utilization. It is seen that the water recovery rate is higher at lower utilization; however, the corresponding make-up water requirements trend in the opposite direction.

Finally, the potential for water recovery diverges as the S/C decreases. Therefore, while initially one would expect that a lower utilization rate is not desirable, it actually yields better potential for recovery at low S/C ratios. This provides for an interesting trade off between O/C ratio and utilization. Comparing Figs. 6 and 3 shows that a utilization of 60% at a S/C = 1.5 and O/C = 1.0 gives nearly the same water recovery as a utilization of 65% at a S/C = 1.5 and O/C = 1.2. In other words, if the fuel utilization changes during operation, then modifying the O/C ratio in the FPS accordingly can maintain the desired water recovery.

In light of the inability to capture 100% of the required water to enable the fuel processor system to be supplied by JP8 only, elevated pressures were investigated to determine where complete capture would occur. Fig. 7 shows the results of water capture potential versus S/C for pressure changes from 1.0 to 2.0 atm for an O/C = 1.0 and a utilization of 0.65. The pressure changes were applied to all units, heat exchangers, reactors and fuel cell. As seen in Fig. 7 at a pressure of 1.0 atm, there is no condition where complete water capture can occur (discussed above) whereas at 2.0 atm, all conditions capture more than the required water, therefore water would have to be discarded. Since elevated pressure requires heavier hardware and more powerful compressors, it is desirable to operate at the minimum pressure where complete water capture can be achieved. That occurs at a pressure of 1.23 atm. Also at this pressure there is a slight decrease in capture potential but for a wide range of S/C ratios (1.25–2.0) it is possible to achieve enough water recovery where the system does not require make-up water.

In Fig. 3 there was shown an increase in water potential at the lower S/C ratios for an O/C = 0.8, however, not for higher O/C ratios. As pressure is increased, the upturn in capture potential for higher O/C ratios, O/C = 1.0 here in Fig. 7, becomes evident. This can be explained in another way by observing what happens as the S/C is increased. Moving from low to high S/C there is more demand for water, which in turn produces more hydrogen. However, the increased hydrogen, after oxidation to water, has only a small effect on the saturation curve. Again, not until much higher S/C ratios, where the

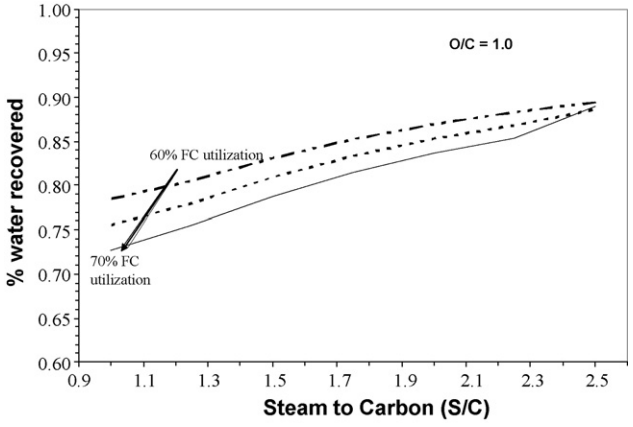

Fig. 6. Water recovery potential for various fuel cell utilization efficiencies for atmospheric, 70 °C operation.

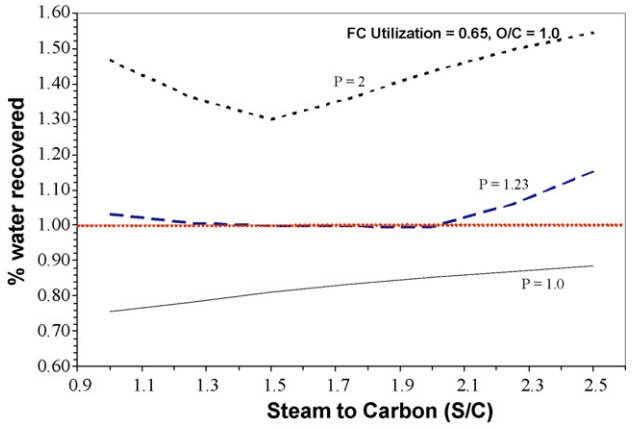

Fig. 7. Water recovery potential for elevated pressures.

exhaust streams are operating near saturation does the capture potential increase again.

Once an optimal pressure of 1.23 atm was identified, the performance over different O/C ratios was investigated. Fig. 8 shows the results of varying O/C for a fuel cell utilization of 0.65 while maintaining operating pressure at 1.23 atm. The O/C = 1.0 is the identical curve from Fig. 7, which is compared to O/C = 0.8 and 1.2 as in the other figures. One noticeable attribute is the way all curves have an upturn at low S/C ratios compared to Fig. 3, in particular O/C = 0.8 sharply increases, more than it did in at 1.0 atm in Fig. 3. In addition, the effect of approaching saturation can now be seen more clearly. At high S/C ratios, the curves begin to rise sharply and are dependant on the O/C ratio. Recall, the higher the O/C ratio, the more combustion occurs in the ATR, thus increasing the water produced. From Fig. 8 it is clear that as O/C increases, because the system is operating very close to 100% recovery, little change can be seen. Therefore, as the O/C increases, the point where saturation occurs moves toward lower S/C ratios.

Because the pressure was optimized for an O/C = 1.0, when the O/C ratio is 0.8, it still dips below the point where 100% water capture can be achieved. To determine whether or not it is advantageous to increase the pressure to enable lower O/C ratios such as 0.8 and to achieve complete capture a trade off must be considered. For example, by lowering the O/C to 0.8, more hydrogen is produced, but higher pressure will be needed to fully capture the required water. The trade off that must be explored is the value that is gained from producing more hydrogen versus increasing the pressure. If an increase in power to a given compressor is required then the system benefits for decreasing O/C would likely indicate doing so. However, if additional or thicker hardware is needed, then likely the benefits would not be there.

In summary, the results of the water balance show that only elevated pressures, above 1.23 atm, will enable complete water capture. The higher the hydrogen utilization in the fuel cell the worse the potential to recover water from the cathode exhaust. If hydrogen generation is the sole objective, then operation at low O/C ratios is best. But if water recovery is the sole objective then higher O/C ratios is preferred. Lastly, the greatest potential for water recovery is to operate a stream near the saturation conditions before going into any heat exchangers.

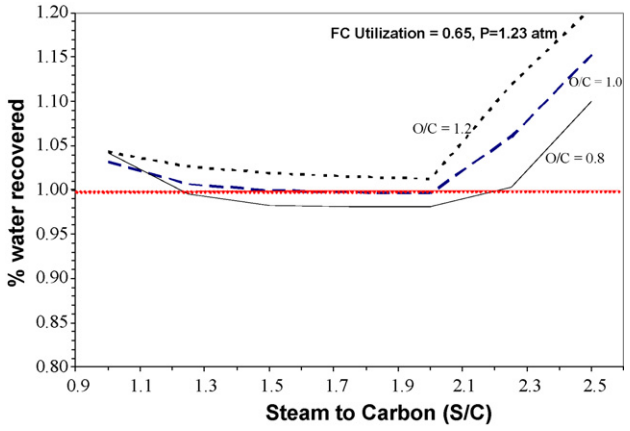

Fig. 8. Water recovery potential for various O/C ratios at $P = 1.23$ atm.

3.2. Energy balance

The energy balance for this system is not nearly as complex as the water balance issue. All simulations conducted resulted in energy being discarded to the environment. In the fuel processor and fuel cell it was rejected as low grade heat, typically 155 °C or 70 °C and for the AGB, heat was rejected at much higher quality. The real issue with thermal integration is that the operating conditions for a majority of the units cannot tolerate high-temperatures. For example, the WGS reactor will not efficiently convert CO to H_2 and the PROX reactors will enter a second, high-temperature steady state where mostly H_2 is consumed as opposed to CO being oxidized [3,5].

Shown in Table 1, a rudimentary energy balance gives an indication into the amount of energy that goes unused. There is about six times more energy produced than is needed, with a great majority coming from the AGB. In fact, nearly all of the energy needed to preheat the reactants to the required inlet for the ATR can be obtained from the inter-reactor heat exchangers (HX-1, HX-2 and HX-3).

To refine the FPS operation the ASPEN model was used to determine the strategy for thermal management throughout the system. The main objective is to provide temperatures as required by the various units in the system. Thermal management was focused initially on the fuel processing subsystem. Since effective ATR operation requires a reactants (fuel, air, and water) preheat temperature of about 250 °C in order to reach the target exit temperature of about 750–800 °C, these inlet streams are regeneratively heat-exchanged with ATR and WGS exit streams to reach the preheat condition while cooling the reformate streams accordingly. Specifically, JP-8 and water feed are delivered to the ATR exit heat exchanger (HX-1), and the air feed for the ATR is delivered to the WGS exit heat exchanger (HX-2). These ATR feed streams, heated to 250 °C, are sufficient to cool the reformate gas to suitable inlet temperatures for both the WGS and PROX.

The ASPEN simulations verified that the thermal energy needed for preheating the ATR reactants is available from within the fuel processing subsystem, thus the heat generated in the anode exhaust gas burner (AGB) is not utilized. The effluent from this burner is cooled with ambient air to condense water for recycle to the fuel processor. The heat generated in the fuel cell reaction is removed via recirculation of liquid water through the fuel cell stack. This liquid coolant also cools the reformate gas from the PROX-2 to approach the fuel cell temperature; heat is removed from the coolant via heat exchange with ambient air in HX-3.

Based on the water and energy balances, an integrated JP8 fuel processor that combines good water recovery with efficient thermal management and practical operating conditions is shown in Fig. 9. This system overall provides a system efficiency of 18.3% for a 600 W net, 750 W gross electrical

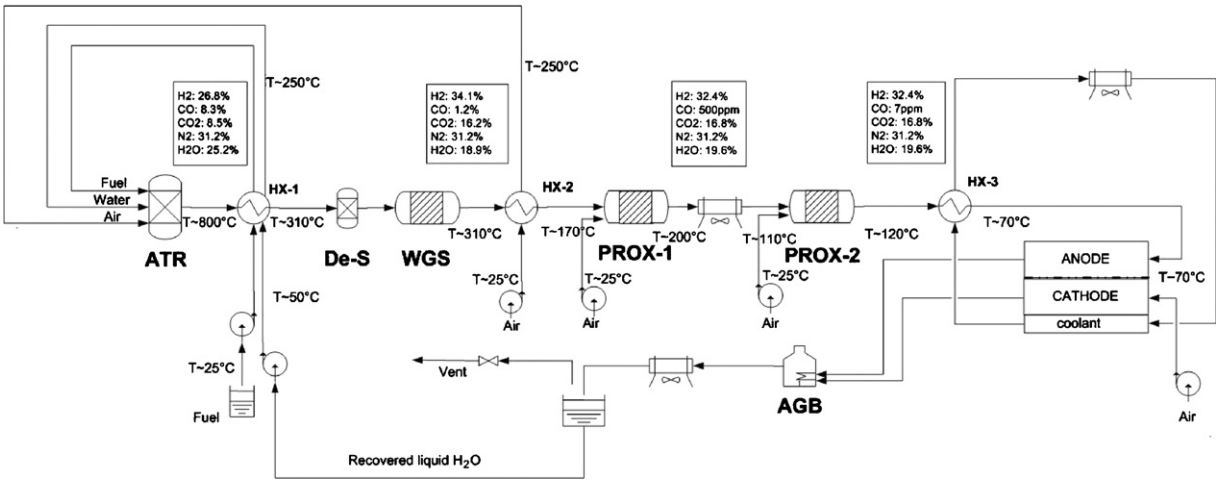

Fig. 9. Final FPS integrated system based on water and energy balances done with ASPEN.

output with a fuel consumption of 0.23 kg/h with 100% water recovery. The main reason for the low efficiency is due to the amount of heat that needs to be rejected to recover the water and the inability to use the AGB exhaust. That is the heat generated by the ATR and WGS reactors is sufficient to preheat the reactants, thus the heat of the AGB is exhausted to the environment.

This system configuration was examined with respect to its effect on water recovery. This scheme eliminates the condenser in the cathode effluent and directs this stream to the AGB, where it serves as the oxidant for the anode effluent stream (using the oxygen that is not utilized in the fuel cell). There is more than enough oxygen in the cathode effluent for this purpose. This approach allows elimination of the air feed device for the AGB. Accordingly, all condensation is carried out in the AGB exhaust stream. The resulting AGB exhaust has a higher concentration of water vapor than there would be should the AGB exhaust and cathode effluent be taken separately. This results in enhanced water recovery rate. At a condensation temperature of 50 °C the water recovery rate at a utilization of 60% is 0.98; the corresponding recovery rate at a utilization of 70% is 0.90. These results indicate the desirability of the modified configuration not only from a water recovery point of view, but also because of system simplification and lower parasitic power.

As already discussed, higher pressure allows the vapor pressure of water to be reached at lower vapor phase mole fractions of H_2O, thereby providing more water to the liquid phase. Quantitatively, operation at an absolute pressure of 1.5 bar would allow complete water recovery at condensation temperatures of 57 and 56 °C for utilization values of 60% and 70%, respectively. Although these condensation temperatures may not be achievable under the most severe ambient temperature conditions, considering practical burdens for heat exchanger size and parasitic power, the system pressure design point of 1.5 bar is considered practical. The pressure could be ramped up (say, within the 1.5–2.0 bar range) to accommodate extreme ambient temperature conditions with regard to water recovery, as necessary.

3.3. Experimental verification

As stated previously the conditions simulated were taken from past experience in operating liquid fuel processing systems as well as from literature. Typically, the ATR operates at high enough temperature where equilibrium at very high space-velocities can be easily achieved. The bigger challenge is the CO clean-up train, especially the single-stage WGS. There have been studies done exploring the operational capabilities of such a configuration [5,6,8,11]. Yet, to ensure the ASPEN simulations were within bounds of practical reactors available today, an integrated CO clean-up train was assembled using rudimentary heat exchangers to achieve the inlet temperatures required for each reactor. The exchangers were considered rudimentary because they were configured in an open loop, where the removed heat was rejected to the atmosphere and not used to preheat any reactants.

Patented short contact-time (SCT) catalyst material was supplied by Precision Combustion Inc. of North Haven, CT for the testing. This made it possible to design, assemble, and demonstrate a functionally integrated subsystem comprising the WGS and PROX reactors and confirming the performance viability of the ultra-compact reactor elements of the type that are targeted for this mission. Experimental apparatus and associated instrumentation were set up to incorporate a single WGS reactor (operating at about 300 °C) and a two-stage PROX reactor (operating in the 140–240 °C range) with intermediate cooling sections. The feed to the WGS simulates the effluent CO concentration of the ATR reactor (about 10%). The nominal target for WGS effluent CO concentration is about 1%, and that for the PROX effluent is about 10 ppm.

A test was conducted whereby the flow rates of the gas species were set via the micro flow-controllers and their concentrations were measured by the micro-GC over a period of time. Following a period of satisfactory exploratory testing with used catalysts the test station was fine-tuned and set up for formal testing of the WGS and PROX individually. After the performance of the individual catalysts and reactors were

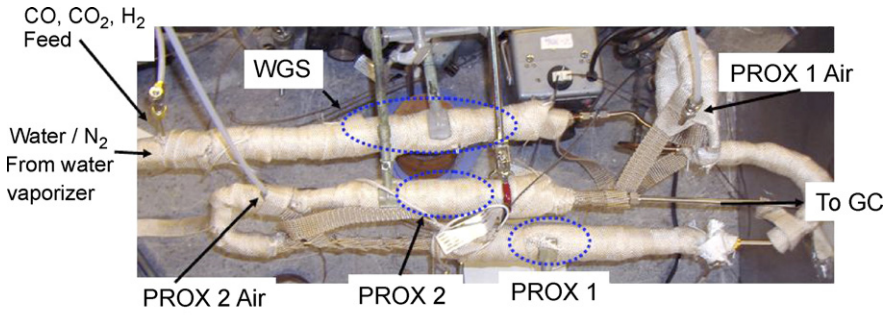

Condition	H_2	CO_2	H_2O	N_2	*CO (ppm)*
A	25	13.8	28	33.2	*8*
B	25	13.9	28	33.1	*9*

Fig. 10. Complete integrated CO clean-up train assembly using catalyst material from Precision Combustion, Inc.

qualified, the two units were physically and functionally integrated, including intermediate thermal management means. The testing of the units individually and as-integrated confirmed the performance capability of the short contact-time (SCT) catalyst elements in allowing ultra-compact and lightweight reactors. The space-velocities used in obtaining the desired conversions were very high; the WGS yielded CO effluent concentrations of about 1% at a space-velocity of over 27,000 h^{-1}, and the PROX yielded less than 10 ppm CO at a combined space-velocity (PROX-1 and PROX-2 together) of 90,000 h^{-1}.

Fig. 10 shows the coupled assembly of the CO clean-up train. The primary system components and flows are identified. The table in Fig. 10 shows the results of the clean-up train achieving less than 10 ppm CO. A more detailed discussion of the results from the testing is in preparation and will be published elsewhere. These results, along with other studies from the literature, provide confidence that the ASPEN® simulations are depicting real operating systems that could be deployed provided the conditions for water recovery discussed above are met.

3.4. Size and weight estimates for the FPS

The kinetic results obtained in this effort were used to estimate the sizes and weights of the fuel processing reactors required for a fuel processor supplying 750 W gross power operating on sulfur-free JP8 fuel. The values of the actual reactors used for the experimental verification discussed above are shown in Table 2. The values for the ATR reactor were estimated from prior experience and are 0.04 L and 0.03 kg. The reactor housings are taken into account in the system size and weight values. Also shown in Table 2 are the estimated heat exchanger sizes and weights for the system that would be used in an integrated fashion, i.e. heating of reactants. These figures were arrived at through heat transfer analysis along with consultation with heat exchanger manufacturers.

The sulfur removal strategy for the JP-8 fueled system is based on prior experience with sulfur-containing diesel and gasoline fuels. It has been found in short-term testing that the sulfur in these fuels does not adversely affect ATR-based fuel processor performance. This is attributed to high-temperature, reducing-atmosphere conditions generated in the ATR. The sulfur compounds in the fuel predominantly tend to form H_2S, and this compound can be absorbed by zinc oxide based materials at lower temperatures. The system design incorporates such an absorbent bed upstream of the WGS for operation at WGS-type temperatures. The sulfur absorption properties of zinc oxide were used in sizing the absorbent bed for a change-out interval of 600 h. This resulted in an estimated volume of 0.5 L and weight of 0.6 kg.

Evidenced in Table 2 there are a few items of interest that provide insight into the units that significantly contribute to the size and weight of a FPS. First, the reactors do not contribute significantly, yet among them the WGS is the largest unit and improvements in WGS catalyst activity would provide the most benefit. Even though the PROX units typically consume some hydrogen while removing the CO, they are a very small fraction of the overall size and weight. The real size and weight penalty come from the heat exchangers, primarily the ones that do not have a large temperature gradient to work with. For example, although the ATR–WGS HeX removes a large wattage, 1.5 kW,

Table 2
Detailed values of an integrated CO clean-up train achieving 100% water recovery

Unit	kW/l	kW/kg	cm^3	L	kg
WGS	6	12	100	0.100	0.05
PROX 1	33	64	18	0.018	0.01
PROX 2	33	55	18	0.018	0.01
Reactor totals			136	0.136	0.07
W removal needed					
ATR-WGS HeX	1528		19	0.019	0.12
WGS-PROX HeX	235		32	0.032	0.39
AGB-HeX	1000		165	0.165	0.63
Cathode conderser HeX	300		32	0.032	0.39
PROX-FC HeX	250		32	0.032	0.39
Heat exchanger totals			280	0.28	1.92
Total CO clean-up train			416	0.42	1.99

it can be small, thus light, because the temperature driving force is between 850 and 350 °C. However, the AGB-HeX are smaller wattage, but must get down to nearly ambient – 50 °C. Therefore, there is a low temperature gradient driving force. Conversely, the WGS to PROX HeX are fairly large due to the small temperature difference that they need to work within, i.e. ∼350–150 °C. It is clear advances in heat exchange technology or innovative ways to manage the heat would yield significant size and weight reductions.

Finally, it should be noted that none of the catalytic reactors were tested for extended periods of time, thus durability or long term activity measures, must be considered. In addition, the presence of sulfur will require larger catalytic reactors due to a reduction in activity. Depending on the quality of the fuel and the robustness of the catalyst, the size and weight of those units can vary considerably.

4. Conclusions

An ASPEN® simulation was conducted to determine the requirements for complete water recovery and thermal management of a JP8 fuel processor. The results indicate that a slight elevation in operating pressure, between 1.25 and 1.5 atm, will enable 100% water recovery over a S/C and O/C operating range of 1.0–2.5 and 0.8–1.2, respectively. An overall efficiency of 18.3% for a 750 W gross, 600 W net FPS was calculated, largely due to the inability to use most of the anode gas burner heat. While the ranges used for the simulation were verified experimentally for the CO clean-up train, it was in the absence of sulfur which will likely increase the size and the weight of the reactors. Finally, for a complete 750 W gross FPS achieving 100% water recovery operating on sulfur-free JP8, the size and weight are estimated to be 0.46 L and 2.02 kg with the bulk coming from heat exchangers working within small temperature gradients.

Acknowledgements

The authors wish to thank Precision Combustion for supplying the catalyst material and Dr. Arthur Kaufman for insightful discussions on the simulation results. Partial funding for this effort was provided by The Office of Naval Research under contract # N00014-05-M-0216.

References

[1] S. Ahmed, J. Kopasz, R. Kumar, M. Krumpelt, J. Power Sources 112 (2002) 519.
[2] S. Ahmed, M. Krumpelt, Int. J. Hydrogen Energy 26 (2001) 291.
[3] M.J. Castaldi, R. LaPierre, M. Lyubovski, W. Pfefferle, S. Roychoudhury, Catal. Today 99 (2005) 339.
[4] S. Roychoudhury, M. Castaldi, M. Lyubovsky, R. LaPierre, S. Ahmed, J. Power Sources 152 (2005) 75.
[5] M.J. Kahlich, H.A. Gasteiger, R.J. Behm, J. Catal. 171 (1997) 93.
[6] M.J. Castaldi, M. Lyubovsky, R. LaPierre, W.C. Pfefferle, S. Roychoudhury, SAE Technical Paper 2003-01-1366 (2003).
[7] N.A. Koryabkina, A.A. Phatak, W.F. Ruettinger, R.J. Farrauto, F.H. Ribeiro, J. Catal. 217 (2003) 233.
[8] W. Ruettinger, O. Ilinich, R.J. Farrauto, J. Power Sources 118 (2003) 61.
[9] W. Ruettinger, X. Liu, R.J. Farrauto, Appl. Catal. B: Environ. 65 (2006) 135.
[10] O. Korotkikh, R. Farrauto, Catal. Today 62 (2000) 249.
[11] X. Liu, O. Korotkikh, R. Farrauto, Appl. Catal. A: Gen. 226 (2002) 293.
[13] C. Bao, M. Ouyang, B. Yi, J. Power Sources 156 (2006) 232.